Dipolar field effects in a solid-state NMR maser pumped by dynamic nuclear polarization

Vineeth Francis Thalakottoor Jose Chacko, Daniel Abergel

Dipolar field effects in a solid-state NMR maser pumped by Dynamic Nuclear Polarization.

Vineeth Francis Thalakottoor Jose Chacko and Daniel Abergel*

Laboratoire des biomolécules, LBM, Département de chimie,

Ecole normale supérieure, PSL University,

Sorbonne Université, CNRS, 75005 Paris, France.

* daniel.abergel@ens.fr

ABSTRACT

We report the observations and the analysis of a pulsed solid state sustained maser generated by proton spins hyperpolarized by Dynamic Nuclear Polarization (DNP) at cryogenic temperatures. Similar unconventional behaviour was observed recently [Weber *et al., Phys. Chem. Chem. Phys., 2019,21, 21278-21286*], with induction decays exhibiting multiple asymmetric maser pulses for short time (100ms) and persistent for tens of second, when the spins are polarized negatively. We present new evidence of such DNP NMR masers, and shed light on previously observed but unexplained features of these masers through simulations of the non-linear spin dynamics using the Bloch-Maxwell-Provotrov (BMP) equations for radiation damping and DNP, and taking into account the (distant) dipolar field.

I. INTRODUCTION

A large magnetization produced by a nuclear spin ensemble, when efficiently coupled to the LCR resonant circuit of the the NMR detection probe, can create a coherent radio frequency (rf) field with significant magnitude. If strong enough, such a field will efficiently act back on the precessing magnetization to rotate the latter back to its equilibrium direction, giving rise to a so-called maser pulse. This well-known phenomenon, improperly termed radiation damping (RD), has been studied decades ago[1, 2] and has motivated a wealth of methodological work aiming at its suppression or control in solution NMR.[3–5] Such a magnetization behavior can also be generated in the solid state, when the spins are brought to a high level of polarization, as has been demonstrated using dynamic nuclear polarization (DNP) at liquid helium temperatures. Even less common is the observation of multiple, self-sustained, maser pulses in the solid state. A few such examples have been observed in the context of DNP at liquid helium[6, 7] or liquid nitrogen [8] temperatures.

This unusual magnetization dynamics is due to the combination of two competing effects, namely, the coupling of the nuclear spins to the detection circuit that generates a radiation feedback field that drives the magnetization back to the $+z$ direction, and known as radiation damping (RD); and an antagonist process that allows to rebuild polarization towards a negative value. In this work, the latter is provided by DNP, when negatively polarized nuclear spins are repolarized by electron spins and possibly also by other nuclear spin species that are also DNP-hyperpolarized but uncoupled to the NMR probe.[9] In this case, the latter nuclear spins represent a reservoir of polarization that is indirectly transferred to the ^{1}H spins through their interactions with the electron spins.

We have recently observed such sustained masers followed by long lasting tails extending over several tens of seconds in DNP-hyperpolarized samples.[7] Following previous analyses of analogous experiments,[6, 9] the experiments were analyzed in classical terms using the nonlinear Bloch-Maxwell equations to take into account the coupling of the magnetization with the detection circuit.[1, 2] In this analysis, DNP was assumed to be in the thermal mixing regime,[10, 11] and described by the Provotorov equations.[12, 13] The combination of both phenomena results in the Bloch-Maxwell-Provotorov (BMP) equations that allow to shed some light onto the unusual nonlinear

magnetization dynamics. However, the BMP esquations are deceptively simple, and are not amenable to an analytical analysis, except in particular cases where analytical solutions of the linearized BMP equations can be derived.[7] Such a study nevertheless provides insight into the non intuitive behaviour of the magnetization dynamics.

Many aspects of this nonlinear dynamics still remain unclear, and not all of them can be explained in the simple framework of the Bloch equations, which calls for a more complete description of the spin system. In particular, in this context, the large magnetization of such highly polarized samples that entails the presence of large distant dipolar fields,[14, 15] contributes to the dynamics of the magnetization. This is unusual in solid state NMR, where dipolar interactions between nuclear spins are of paramount importance, but have no other effect on the magnetization dynamics other than a fast decoherence, therefore a large line broadening[16, 17] with line widths of tens of kHz. In contrast, possible effects of distant, much weaker, dipolar interactions, requires the persistence of coherent magnetization on a much longer time scale. The effects of the associated distant dipolar field (DDF) has been studied in the particular context of solid ^{3}He in a seminal paper by Deville *et al.*.[18] In that work, the unusual long transverse relaxation time allowed to observe such effects. These were subsequently investigated mainly in solution NMR, where the combination of radiation feedback and the distant dipolar field have been the subject of a number of studies. Thus, the combination of both these effects have been shown to produce complex magnetization dynamics, such as spin turbulence[19] and spectral clustering.[20–22]

In typical solid state NMR samples, short NMR decoherence times prevent the development of dynamical effects of the distant dipolar field (DDF), and to our knowledge, no study of the combined collective effects of radiation feedback and the distant dipolar field have been investigated in this context. Here, we explore the dynamics of a magnetization subject to these combined effects in the context of DNP-hyperpolarized spins at liquid helium temperatures, both numerically and experimentally. We provide evidence for the manifestation of the DDF at long evolution times of the magnetization and show that the fine features of the observed maser pulses can be related to the interplay between the latter and radiation feedback.

II. EXPERIMENTAL OBSERVATIONS

TEMPOL, because of its broad EPR resonance line typical of nitroxides, efficiently polarizes nuclear spins with large gyromagnetic ratios, such as ^{1}H, and was therefore used as the polarizing agent. All the experiments were performed on fully protonated compounds and with large volume (800μL) samples containing a mixture of 250 μL H_2O, 400 μL unlabelled Glycerol, and 50 mM of the TEMPOL radical obtained from a 150 μL stock solution. DNP experiments were performed in a Bruker prototype DNP polarizer operating at a magnetic field of 6.7 T and at a temperature of $\sim$ 1.27 K. Microwave (μw) irradiation was provided by an ELVA1 source emitting around 94 GHz, coupled to a Virginia Diodes (VDI) frequency doubler to achieve irradiation at a frequency $\nu = 188.38$ GHz for negative nuclear polarization. The absence of deuteration of the compounds is unusual for DNP experiments, but turned out to be necessary to obtain sufficient sample magnetization in our setup, therefore significant radiation feedback. This can be explained by the moderate quality factor $Q \approx 127$ of the probe used for NMR signal detection at 1.2K. (full width at -3 dB was 2.23 MHz, measured at 285.325 MHz), as well as the limited power of the μw source used for these experiments ($\approx$ 32 mW) In all experiments performed in this study, the μwave frequency was set so as to polarize nuclear spins negatively. For the buildup experiments, nuclear spins were saturated by a train of hard 90^o pulses. The μwave source was subsequently turned on and the sample was continuously irradiated. Short and low-power pulses (pulse power = 123.5 μW; pulse length = 8 μs, flip angle = 0.1^o) were used to achieve small flip angle read pulses every 5 seconds for signal buildup monitoring. In the maser experiments, the nuclei were also initially saturated by the same train of hard rf pulses. Then μwave irradiation of the electron Zeeman spin transition was turned on for nuclear magnetization buildup, but no rf monitoring of the signal was used in this case and the system was let to polarize for $\sim$ 40 min, a duration sufficient to ensure a stationary state of the nuclear polarization in these experimental conditions. This period was followed either by a single, low power, short rf pulse to trigger radiation damping, or by no rf pulse at all. Radiation damping was thus triggered either by short and low power pulse (8 μs at 1.23 μW) with a small initial flip angle (0.01^o), or by spin or electronic noise. The signal was subsequently observed, without any further radiofrequency excitation, but in the presence of continuous μwave irradiation.

A. DDF in the "linear regime": line narrowing and line shifts

A shift of the NMR line proportional to the z component of the magnetization caused by the presence of a strong dipolar field is a well documented phenomenon and is observed in NMR of liquids.[15, 23, 24] In the case of hyperpolarized solids the line shift effect due to the dipolar field is usually rationalized through the theory of moments.[11, 25] Indeed, a direct measurement of the ^{1}H line shift is difficult and inaccurate in these DNP experiments because the determination of the location of the maximum intensity is prone to large errors on such broad and possibly non symmetrical lines. [26] Therefore, the first moment, or center of gravity of the resonance line provides a measure of the NMR line shift, which is identical to the shift of its maximum in the case of a symmetrical line shape. It is defined as:

$$M_1 = \int_{-\infty}^{\infty} \omega f(\omega) d\omega \ , \tag{1}$$

where $f(\omega)$ is the normalized NMR lineshape function.

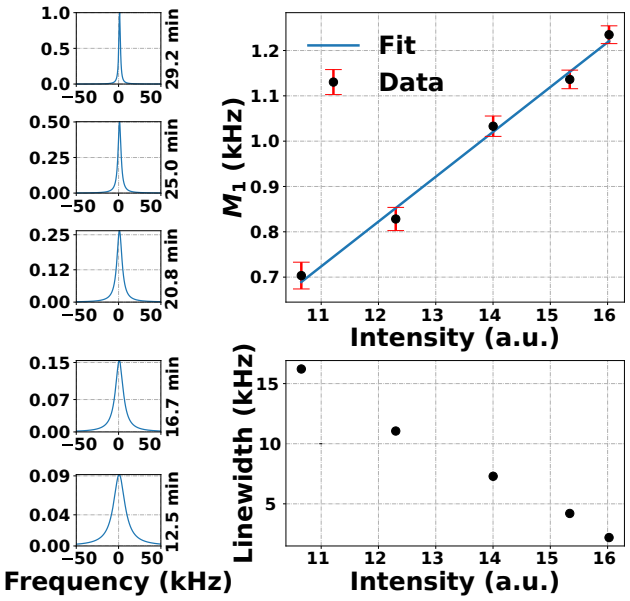

FIG. 1. Line narrowing and line shifts upon DNP buildup. Left: the resonance line widths are respectively 16100 Hz, 11300 Hz, 5700 Hz and 4330 Hz from bottom to top. Right: experimental first moments of the line M_1 vs line intensity. Filled symbols denote values extracted from experimental spectra; the straight line indicates the linear fit of the data (see text for details).

The first moment of the ^{1}H NMR line was computed at different times of the buildup experiment. However, at low polarization levels, the spectral line has not returned to baseline at the edges of the spectral window (± 50 kHz about the carrier). Therefore, in order to avoid numerical errors due to the truncation of the tails of the NMR reso-

nance lines, the first moments M_1 were numerically fit to a numerical model. Using a Lorentzian shape appeared acceptable for such symmetrical lines. And for consistency, the same procedure was also used for narrower resonance lines obtained for higher polarizations. The changes of the first moment upon increase of the signal intensity during a buildup experiment are depicted in Figure 1. The graph clearly shows the linear dependence of the first moment with the line intensity, therefore the polarization and the magnetization.

Interpreting the observed changes of M_1 computed from the NMR line requires a model of the magnetic interactions governing the dynamics. In the problem at hand, these include the spin dipole-dipole interactions and the spin coupling with the probe through radiation feedback. However, because the spins are on resonance with the probe, radiation feedback induces no frequency shift.[2] The latter is thus only caused by the presence of the dipolar field. Consequently, in these experiments, the first moment can indeed be related to the spin polarization, therefore magnetization, in the sample. During the buildup experiment that led to the spectra of Fig. 1, the electron polarization is in a steady state, so that the shift of the resonance line, measured by the first moment, varies linearly with the nuclear (^1H) z magnetization. In the DNP sample, the shift of the nuclear first moment is due to the local dipolar fields generated by both the nuclei and the paramagnetic impurities.[11, 27] Thus, M_1 is the sum of the respective contributions of the nuclear and electrons, $M_1^{nn} = \frac{2}{3}\mu_0 I\gamma_{\mathrm{H}}^2\hbar\xi N_h P_h$ and $M_1^{ne} = \mu_0 S\gamma_h\gamma_e\hbar\xi N_e P_e$,[11, 27, 28] where I, S are the nucleus and electron spins, N_e and N_h their densities, and P_h and P_e their concentrations. The shape factor $\xi = \frac{3}{8\pi N_h}\overline{\sum_i \frac{1-3\cos^2\theta_{ij}}{r_{ij}^3}}$ can be calculated for different sample shapes, and takes the simple values ($\xi = 0, -1/2$ for a sphere or an infinitely long cylinder).[27]

In contrast, the computation of the second moment cannot be related to the line narrowing observed upon DNP polarization (see Fig. 1, where the line width drops from ~ 16 kHz to ~ 4300 Hz). Indeed, The expression of the second moment derived in the literature[25, 29] is based on a dynamical model where the spins are subject to a hamiltonian that accounts for the nuclear and electron-nucleus dipole dipole interactions, and where the dynamics are described by a Liouville equation. However, in the presence of radiation damping, the quantum description of the process is more involved, as it would require to consider the complete {spin+field} system, and a dissipative relaxation operator for the field, which leads to a nonlinear Liouville equation for the spins (see for a discussion Ref. [30]). In this case, the theory of moments derived in the case of spin-

spin interactions (as in Ref.[25] for instance) does not apply and, to our knowledge, no similar treatment has been proposed.

The width and shape of the resonance line strongly depend on the radiation feedback from the probe that maintains a phase coherence between the spins, so that the expressions derived in the literature for the second and higher moments for the case of dipolar interactions do not apply. Thus, the decrease of the line width with increasing magnetization (Figure 1) is a first manifestation of the qualitative change of dynamics induced by radiation feedback from the probe upon hyperpolarization, and illustrates its interference with dipole dipole interactions between nuclear spins.

B. Observation of pulsed masers

A high nuclear polarization state was achieved by irradiating the sample with the μw source without signal monitoring so as to avoid perturbation of the ^{1}H magnetization by radiofrequency pulses, during a period of time determined from preparatory buildup experiments. This buildup time was set to 40 min. Signal acquisition then started and lasted typically for tens to thousands of seconds, during which the sample was under continuous μw irradiation. This experimental procedure led to consistent observations of multiple maser pulses. In the example shown in Figure 2, the induction signals were obtained on a total duration of 4000 s. In order to handle these large data sets, the signal was acquired in a pseudo-2D fashion as a series of 200 scans of 20 s each, where a single rf pulse only was used at the beginning of first scan to trigger radiation damping. All other induction signals were acquired under μw irradiation, and no further rf pulse was applied.

As shown in Figures 2(a)-2(b), these signals exhibit long series of maser bursts of approximately constant intensities and regularly spaced, except for the very first one. This first maser burst immediately follows the trigger rf pulse, its peak intensity is roughly ~ 10 times larger and its duration accordingly shorter, than those of the next maser pulses. This feature is reproducible in all the experiments giving rise to sustained masers. Besides, and although such sustained maser pulses were easily reproduced, their duration and the delay between them could vary between different experiments in an uncontrolled way. A striking feature of the observed sustained masers is the absence of decay of the maser pulse intensities with time (except for the initial one), suggesting that the magnetization reaches a pseudo-periodic asymptotic dynamics kind of regime.

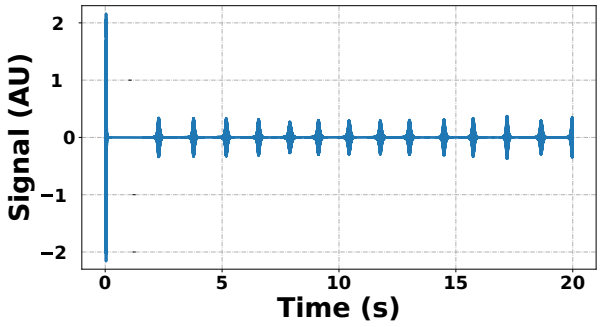

(a)

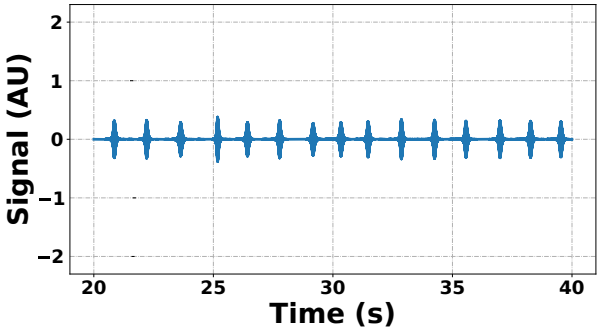

(b)

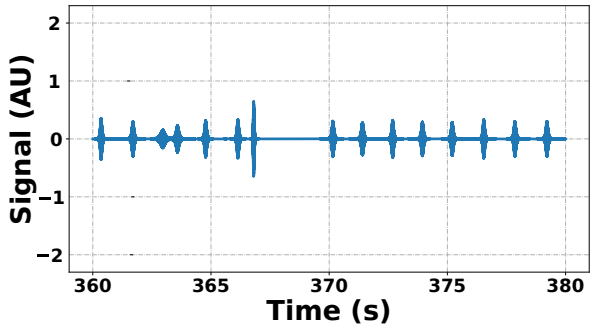

(c)

FIG. 2. Sustained maser upon continuous μw irradiation. 2(a),2(b) and 2(c) are the 1^{st},2^{nd} and 19^{th}, 20 s extracts of a single $200 \times 20s$ induction signal collected as a pseudo-2D experiment. No rf pulse was applied, and the sustained maser sequence was triggered by noise . Most of the FIDs show an evenly spaced succession of maser bursts (2(a),2(b)). However, on few instances, spurious maser pulses were also observed (2(c))

However, some irregularities appeared in these experiments, with the appearance of maser pulses of various widths and at random delays between them.2(c) However, in all our experiments, these were transient behavours that never led to a chaotic dynamics.

Moreover, it is important to realize that, between the maser pulses, the detected signal, although weak, is never below the noise in these experiments. This is shown in Fig 3. This suggests that in this sequence, maser bursts are not triggered by noise, but by

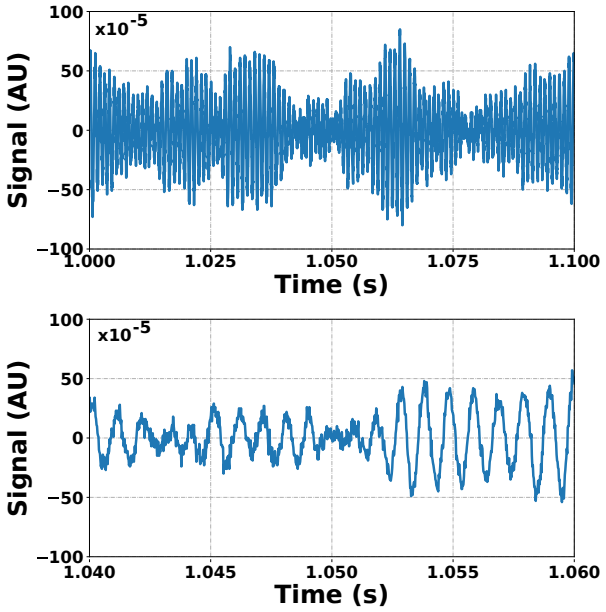

FIG. 3. Enlarged view of the 100 ms region starting at 1 s of the induction signal of Fig. 2(a). The signal remains significantly above the noise level between consecutive maser pulses, indicating the persistence of magnetization coherence throughout the experiment (the same vertical scale as in Fig. 2 is used) .

the persistent coherent in-plane magnetization throughout the experiment. It is worth mentioning the orders of magnitude of the time scales involved in these experiments. Indeed, not only the maser pulses were separated by delays on the order of the second, but also their duration were on the order of ~ 200 ms, as shown in Fig. 4(b). As mentioned above, the first maser was shorter, with a total duration of ~ 50 ms (see Figure 4(a)). Therefore, applying a Fourier transformation to the decaying part of the pulse, one obtains an narrow line. This is exemplified by the spectrum obtained after processing the maser pulse occurring around 2.3 s in Figure 2(a). The obtained line width is ~ 10 Hz, a rather unusual value for a non rotating solid (Fig.4(c), and significantly smaller than the dipolar line width.

C. Some manifestations of the dipolar field

A closer look at these bursts (Figure 4(a) and 4(b)) allows to identify additional features. Indeed, one notices that the envelope of these maser pulses show an asymmetric profile, with a faster rise than decay, a characteristics that is not explained by a simple Bloch-Maxwell equations of the radiation feedback theory.[2, 31] Moreover, the frequency offset of the signal with respect to the carrier frequency is not constant over

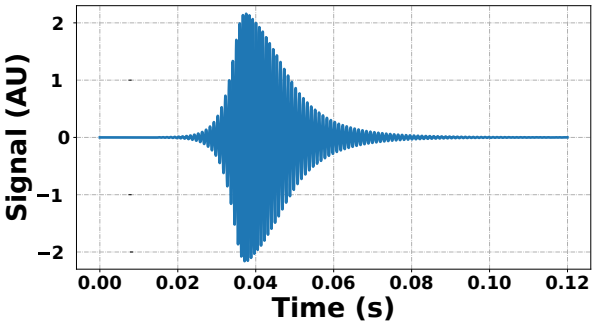

(a)

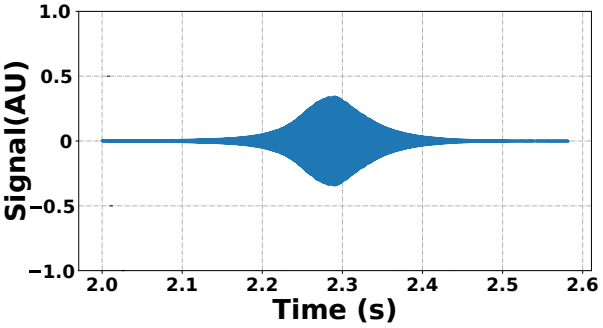

(b)

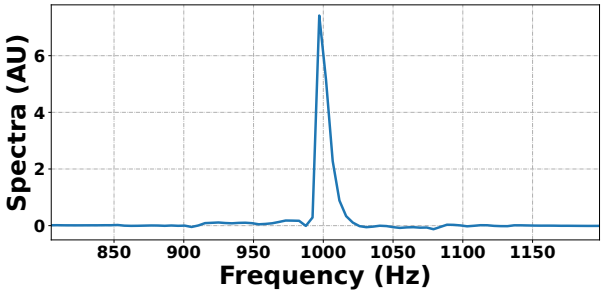

(c)

FIG. 4. 4(a) and 4(b) are the first and second maser bursts of the experiment depicted in Figure 2(a). In 4(a) , the asymmetry of the maser is apparent. In 4(c) the Fourier transform of the decaying part of the maser in 4(b) shows a line width reduction to ~ 10 Hz. The spectrum was obtained after Fourier transformation of 10380 points starting from the top of the maser burst. No zero filling was used. Induction decay signal was acquired every 20.0 μs.

time, which can be seen by superimposing time traces of different bursts and comparing the periodicity of the signals. Mere visual inspection of such a superposition, depicted in Fig. 5 for the first fives maser pulses of Figure 2(a), shows a shorter period during the first maser pulse than during the next ones. This phenomenon can be ascribed to the presence of the DDF, the manifestations of which have already been described above, further investigated by numerical simulations in the following.

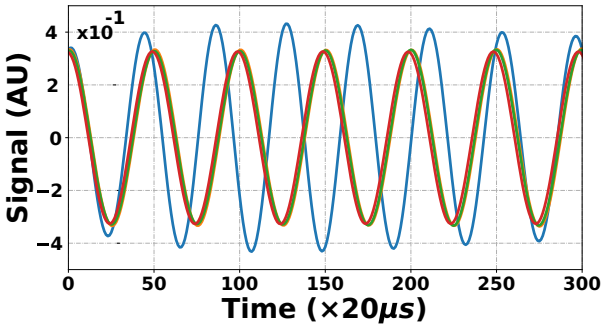

FIG. 5. Resonance frequency shifts due to the dipolar field - Extracts from the first (blue), and three subsequent maser bursts of the induction signal depicted in 2(a) are shown. Superposition of the time signals clearly shows that during the same time interval, the first signal exhibits 7 periods and the subsequent ones only 6 (the first MASER has been scaled down for visualization).

1. Observation of Chirped maser pulses

Further dramatic manifestations of the frequency shift caused by the dipolar field were also observed. One such example is shown in Fig. 6(a), where the induction signal has a quasi rectangular profile that lasts several tens of ms, quite remote from the typical (or approximately) hyperbolic secant maser pulse envelope. These signals exhibited time-varying frequency, giving rise to a squared chirped maser pulse, and a simultaneous slight decaying intensity preceding an abrupt return to zero of the signal amplitude. A time-frequency analysis of this FID based on the short-time Fourier transform[32] depicted in Fig. 6(c) shows the frequency change with time during the pulse. The frequency shift between the beginning and the end of the pulse was about 7500 Hz. The combined resonance and intensity changes are characteristic of the presence of the DDF,[33] and such induction signals are yet a surprising manifestation of nonlinear dynamics of the magnetization in the simultaneous presence of a strong dipolar field and an efficient radiation feedback.

D. Comparison with previous experimental results

Our observations are in line with previous work[7, 9] in many respects, but also show strikingly specific features. In ref.[7] the induction signals consistently exhibited a short series of $\sim 2-4$ ms maser pulses separated by delays of decreasing duration for ~ 100 ms, followed by monotonously decaying signal for tens of seconds, without further maser pulses. No such signals were observed here, where, in contrast, all the observed sustained maser series were of the kind shown in Figure 2, without damping

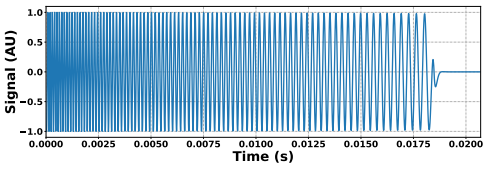

(a)

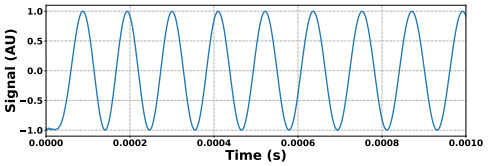

(b)

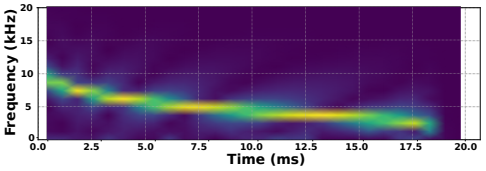

(c)

FIG. 6. Unexpected "square" maser chirped burst observed in a DNP-NMR maser experiments. The shape of the signal differs dramatically from the typical hyperbolic secant kind of envelope of the maser bursts (6(a)): a $\sim$ 18 ms induction signal with an only slightly decaying intensity and ending abruptly was observed. Fig. 6(b) shows an enlarged view of the first oscillations of the induction signal. The increasing period of oscillation is apparent on the induction signal and evidenced by a time-dependent Fourier transform analysis of the induction signal (6(c)). Pulse power was 0.123 mW, pulse length 8 μs, for a $\sim 0.1^{o}$ flip angle. The time-frequency analysis was performed using the STFT (Short Time Fourier Transform) method [32]. The spectrogram shown was obtained through the Scipy implementation of the STFT method (scipy.signal.spectrogram).

of the pulse intensities. These discrepancies are quite puzzling, but some significant differences between experimental conditions in which experiments were performed here and in ref. [7] should be pointed out that may help their interpretation. Here, experiments were performed with a probe of moderate Q, so that radiation damping was less efficient. Therefore, in order to achieve a large enough magnetization, larger volume samples were used (800 μL instead of 150 μL used in our dissolution-DNP setup) and only unlabelled (non deuterated) compounds were used for the sample preparation in order to increase the ^{1}H density. We found that these conditions were necessary to generate MASER pulses. Besides, the complete absence of ^{2}H nuclei in the sample precluded repolarization of ^{1}H through a cross-talk mechanism,[34–36] in contrast with our previous study.[7] Finally, MASER pulses were not observed in the absence of continuous μw irradiation, which was deemed necessary in all cases in the present study. This is explained by the absence of deuterium in the sample, which is not coupled to

the probe but serves as a repolarization reservoir for ^{1}H.[7]

III. THEORETICAL HYPOTHESES AND NUMERICAL MODEL

A. Model

The above suggests that dipolar field effects are effective in the magnetization dynamics of the experiments presented here and, therefore, the simple four-dimensional model of the BMP equations misses some of the observed features of the dynamics. Providing a detailed and effective model of the collective dynamics of a spin ensemble subject to the combination of radiation feedback from the probe, dipolar field effects and DNP is a complex task. However, one is only interested in the dynamics of a classical magnetization, so that the entire system can be described in terms of interacting classical magnetic moments. Nevertheless, even with such a drastic simplification, the complexity of this system requires further simplifications and hypotheses. In solids, dipole-dipole interactions provide an efficient mechanism for decoherence, leading to FIDs of a few hundreds of microseconds. This is particularly effective for near neighbor interactions, where dipolar coupling is strong. Alternatively, because the dipolar interactions fall off relatively fast as $\sim r^3$, these effects may assumed much weaker at long distances, where the interaction energies are smaller and the associated time scales accordingly longer. Therefore, we here assume that the environment of each spin i is decomposed as follows. A small region centered on i, the dimensions of which are large with respect to the first neighbor distances but much smaller than the sample dimensions, is responsible for decoherence and the fast decay of the NMR signal. Alternatively, the long distance, and accordingly weaker, interactions with remote spins affect the magnetization dynamics only on time scales that are much longer than the typical inverse line width. Therefore, except for a contribution to the resonance frequency, this DDF is not expected to affect the magnetization dynamics. This may nevertheless be the case if phase coherence between spins is maintained long enough, as in the presence of a strong radiation feedback. These considerations lead us to envisage a simplistic model where all the spins in the system have a common T_2 relaxation time (and a $\gamma_2 = T_2^{-1}$ rate) that represents the effect of the local dipolar interactions. Alternatively, the dipolar contribution from remote spins, an active ingredients of the magnetization dynamics in this context, is treated explicitly. In this model sample, the magnetic moments are

sitting on a regularly spaced lattice and the local dipolar field at site i, $\mathbf{B}_d(\mathbf{r}_i)$, due to the long range dipole dipole interactions can be explicitly computed for all moments in the model sample as:

$$\mathbf{B}_d(\mathbf{r}_i) = \frac{\mu_0}{4\pi} \sum_j \frac{3[\mathbf{m}(\mathbf{r}_j).\hat{\mathbf{r}}_{ij}]\hat{\mathbf{r}}_{ij} - \mathbf{m}(\mathbf{r}_j)}{|\mathbf{r}_i - \mathbf{r}_j|^3} \tag{2}$$

In these equations, $\mathbf{m}(\mathbf{r}_i)$ and $\mathbf{m}(\mathbf{r}_j)$ are the moments at sites i and j, and $\hat{\mathbf{r}}_{ij} = (\mathbf{r}_i - \mathbf{r}_j)/|\mathbf{r}_i - \mathbf{r}_j|$ is the unit vector joining the positions i and j. Another essential ingredient of the theoretical setup is the presence of the radiation feedback field from the coil and acting on the nuclear spins. The coupling of the spins with the circuit induces a feedback radiofrequency field $\mathbf{B}_{rd}$ that obeys Kirchhoff equations.[1, 2] Assuming a homogeneous rf field in the sample, this radiation feedback field is given by:

$$\mathbf{B}_{rd} = \int_V G\, \mathbf{m}_+(\mathbf{r}) e^{-i\psi} d^3r \tag{3}$$

where V is the sample volume, and the strength of spin-coil coupling is given by $G = \frac{\mu_0}{2}\eta Q$, where η, γ_{H}, Q, and μ_0 are respectively the filling factor, the gyromagnetic ratio, the quality factor and the vacuum permeability. The corresponding radiation damping rate is [2] $\gamma_{rd} = \frac{\mu_0}{2}\gamma_{\mathrm{H}}\eta Q m_0$, where m_0 is the magnitude of the average magnetization density:

$$\mathbf{m}_0 = \frac{1}{V}\int_V \mathbf{m}(\mathbf{r}) d^3r. \tag{4}$$

The phase factor ψ depends on the impedance of the {spins + coil} circuit and its expression depends on the electrical model of the setup.[2, 37] When the Larmor frequency of the spins exactly matches the probe natural frequency, $\omega_0 = \omega_{\mathrm{LC}}$, then $\psi = -\pi/2$, and the radiation feedback field lags the in-plane magnetization by 90^o.

The last ingredient of the dynamical model is the DNP hyperpolarization process of the nuclear spins, which provides the magnetization build-up mechanism. In our experiments, performed at or below 4 K with TEMPOL radical concentrations above 50 mM, DNP is assumed to be in the thermal mixing regime,[35] a process described by the Provotorov equations.[12, 13, 38, 39] In this thermal mixing description, electron-electron and electron-nuclear spin interactions are associated to several coupled energy reservoirs, each of which characterized by a spin temperature T_i (or its inverse $\beta_i = 1/k_{\mathrm{B}}T_i$). Thus, Nuclear Zeeman (NZ) and electron dipole-dipole, non Zeeman, (eeD)

reservoirs are in thermal contact with each other,[10, 11, 40, 41] and when several nuclear species are present, each one constitutes a distinct reservoir coupled to the eeD reservoir, hence indirectly to one another,[34, 35] adding further complexity to the associated Provotorov rate equations.

We recently proposed a simplified model[7] to empirically capture the effect of DNP on the collective and macroscopic aspects of the nuclear spin dynamics, and to reproduce experimental observations. In this model, the nuclear inverse spin temperature β_n of the ^{1}H Zeeman reservoir relaxes exponentially with time constant $\gamma_{n,ee}$, to the electron non-Zeeman spin temperature β_{ee}, which also exponentially relaxes (with rate γ_{st}) to a stationary value that represents either its polarization upon μw irradiation, or the lattice temperature. This toy model of DNP is relevant to the case where ^{2}H nuclei are present in large quantities in the sample, as these provide a source of polarization to the ^{1}H nuclei by an indirect "cross-talk" mechanism through their interaction with the electron non Zeeman reservoir.[34–36] Thus, the deuterium spins contribute to the repolarization of the protons and buildup of the nuclear magnetization, and compensate at least partially the ^{1}H Zeeman energy lost to the probe through radiation damping. In this model setup, the z component of the nuclear spin magnetization density at point $\mathbf{r}$, $\mathbf{m}_z(\mathbf{r},t)$, therefore tends to the time-varying value $\mathbf{m}_{oz}^{th}(\mathbf{r},t)$, that "relaxes" to a stationary value $m_0^{st}(\mathbf{r})$. Again, the quantity $m_0^{st}(\mathbf{r})$ pertains either to the stationary value of the ^{1}H magnetization upon μw irradiation, or to its thermal equilibrium, when μw irradiation is turned off. This model therefore writes:

$$\frac{d\mathbf{m}_z(\mathbf{r},t)}{dt}(\mathbf{r},t) = -\gamma_{n,ee}\left[\mathbf{m}_z(\mathbf{r},t) - \mathbf{m}_{oz}^{th}(\mathbf{r},t)\right] \tag{5}$$

and:

$$\frac{d\mathbf{m}_{oz}^{th}}{dt}(\mathbf{r},t) = -\gamma_{st}\left[\mathbf{m}_{oz}^{th}(\mathbf{r},t) - m_0^{st}(\mathbf{r})\right] \tag{6}$$

In Eq. 5, $\mathbf{m}_z(\mathbf{r},t)$ is related to the spin temperature β_n of the ^{1}H:

$$\mathbf{m}_z(\mathbf{r},t) = \frac{\gamma_n^2\hbar^2\mathcal{N}_{\mathrm{H}}B_0}{4k_b}\beta_n(t) \tag{7}$$

where $\mathcal{N}_{\mathrm{H}}$ is the proton spin density; and β_n itself relaxes to the temperature of the eDD

reservoir $\beta_{ee}(t)$, so that one has:

$$\mathbf{m}_{oz}^{th}(\mathbf{r},t) = \frac{\gamma_n^2\hbar^2\mathcal{N}_{\mathrm{H}}B_0}{4k_b}\beta_{ee}(t) \tag{8}$$

This model, introduced in ref. [7], will be referred to as model (A). In the experiments discussed in this work, however, only ^{1}H are present, and once polarized, ^{1}H can only be repolarized from direct interactions with the electrons, under μw irradiation. Therefore, it is assumed that the nuclear spin magnetization density at point $\mathbf{r}$, $\mathbf{m}_z(\mathbf{r},t)$, builds up exponentially towards its stationary value $m_0^{st}(\mathbf{r})$, taken in this case as the stationary polarization level obtained by DNP, with the time constant $\gamma_{n,ee}$:

$$\frac{d\mathbf{m}_z(\mathbf{r},t)}{dt}(\mathbf{r},t) = -\gamma_{n,ee}\left[\mathbf{m}_z(\mathbf{r},t) - m_o^{th}(\mathbf{r})\right] \tag{9}$$

This will be referred to as model (B).

Finally, in the classical and empirical model proposed here, the modified Bloch-Maxwell equations obeyed by the magnetization are:

$$\begin{aligned}\frac{d}{dt}\mathbf{m}(\mathbf{r},t) &= \gamma\mathbf{m}(\mathbf{r},t)\times(\mathbf{B}_{rd}(t)+\mathbf{B}_d(t)) - \gamma_2(m_x(\mathbf{r},t)\hat{\mathbf{x}} + m_y(\mathbf{r},t)\hat{\mathbf{y}}) \\ &- \gamma_{n,ee}(\mathbf{m}_z(\mathbf{r},t)) - \mathbf{m}_{oz}^{th}(\mathbf{r},t))\hat{\mathbf{z}}\end{aligned} \tag{10}$$

where, for model (B), $\mathbf{m}_{oz}^{th}(\mathbf{r},t)$ is replaced by its constant value $m_o^{th}(\mathbf{r})$. Numerical simulations of Equation 10 allows one to study the time evolution of the total magnetization, and provide better insight into the largely non intuitive dynamics of this non local and nonlinear system.

B. Numerical simulations

Numerical simulations aimed at better understanding the possible role of the dipolar field in the experiments presented here, and also in previous work.[7] In all simulations, classical moments with magnetization density $\mathbf{m}(\mathbf{r}_i)$, were located at fixed positions on a grid. In this coarse grained representation of the sample, each moment represents a "cluster" of spins undergoing decoherence resulting from the strong, local dipolar interactions within the cluster, and characterized by a unique relaxation rate γ_2 for all clusters, and given in Equation 10. In addition, the different clusters ($i \neq j$) mutually interact through long-distance dipolar interactions, where the dipolar field at the locus

of $\mathbf{m}^i$ and resulting from its interactions with the magnetization moments $\mathbf{m}^{j\neq i}$ in the sample is written as:

$$\mathbf{B}_d(\mathbf{r}_i) = \frac{\mu_0}{4\pi} \sum_{j\neq i} \frac{1-3\cos^2\theta_{ij}}{2\left|r_{ij}\right|^3} \times [3m_z(\mathbf{r}_j)\hat{z} - \mathbf{m}(\mathbf{r}_j)] \tag{11}$$

where, in Equation 11, the secular approximation part of equation 2 for large $\mathbf{B}_0$ has been assumed (see Ref. [15] for a general discussion). The distant dipolar field is a non-local quantity, making its computation difficult. However, as has been recognized long ago,[18] Equation 11 has the form of a convolution in the real space, so that its Fourier transform with respect to the spatial coordinates is local quantity, which is expressed as a product in the reciprocal space.[18] In terms of the three-dimensional Fourier transforms $\mathbf{B}_d(\mathbf{k}_i) = \int d^3r \exp(i\mathbf{k}_i \cdot \mathbf{r})\, \mathbf{B}_d(\mathbf{r}_i)$ and $\mathbf{m}(\mathbf{k}_i) = \int d^3r \exp(i\mathbf{k} \cdot \mathbf{r})\, \mathbf{m}(\mathbf{r}_i)$, of the dipolar field and magnetization, $\mathbf{B}_d(\mathbf{k}_i)$ is written as:

$$\mathbf{B}_d(\mathbf{k}_i) = \frac{\mu_0}{6}\left[3\left(\hat{\mathbf{k}}_i \cdot \hat{\mathbf{z}}\right)^2 - 1\right] \times [3m_z(\mathbf{k}_i)\hat{\mathbf{z}} - \mathbf{m}(\mathbf{k}_i)] \tag{12}$$

This expression can be numerically computed using the strategy introduced by Enss *et al.*[33] Numerical simulations were performed on an ensemble of spins located on a regularly spaced cubic lattice, with the shape of either a thin disk ($21 \times 21 \times 7$ grid points) or an elongated cylinder ($11 \times 11 \times 21$ grid points). In order to avoid numerical artifacts due to the periodicity induced by the FFT, zero padding was applied.[15, 33] Satisfactory conditions were obtained by increasing the padding dimensions in test simulations until no significant changes on computed magnetization trajectories were observed. The retained padding was $100 \times 100 \times 150$ padding in the x, y, and z dimensions for all simulations. Finally, because of the singularity at $\mathbf{k} = 0$ this component was computed from the average magnetization.[15, 33] Equations 10 were numerically solved using explicit Runge-Kutta method of order 8 [42] implemented in Scipy[43] by the scipy.integrate.solve_ivp adaptive stepsize integrator. The simulations shown in this article were run on a on 10-core Dell Precision 5820 desktop computer.

We used an idealized initial state in which all moments $\mathbf{m}_i$ have the same initial value $(0, -m_o\sin(\phi), m_o\cos(\phi))$, where m_o is the magnitude of $\mathbf{m}_i$ and ϕ is the initial flip angle, which was set to -1^o. The control parameter of the dipolar field effects in our simulations was the magnetization density parameter m_o, which can be related to the average dipolar field ω_{dip} at equilibrium: $\omega_{dip} = \gamma_H \mu_0 \frac{2m_0}{3}$ for a disk-shaped sample and

$\omega_{dip} = \gamma_H \mu_0 \frac{2m_0}{6}$ for a cylinder.[15]

Using these numerical tools, we performed simulations of the magnetization dynamics that follows an initial period of spin DNP-hyperpolarization ending by a small trigger pulse, for models (A) and (B) above that pertain to different experimental conditions, namely, DNP samples composed of a mixture of ^{1}H/^{2}H, or of protons only.

Sustained masers under μw irradiation - ^{1}H only (model B) In a first round of simulations we investigated situations described by model (B), an idealization of the experiments presented above. In order to ensure the presence of maser pulses in the simulations, we set the condition $\gamma_2/\gamma_{rd} \leq 1$ at the initial time of the trajectory, when the magnitude of the total magnetization is largest. The latter was equal to the stationary hyperpolarized magnetization m_0^{st}, which was set to a negative value, as only a negative polarization is expected to lead multiple masers.

In Figure 7, the traces of the magnitude of the transverse magnetization, $\sqrt{m_x^2(t) + m_y^2(t)}$ (red) and of the m_z component of the magnetization are shown. The typical multiple maser pattern is recovered, and is understood to be due to the presence of two antagonist processes, namely, the radiation feedback that rotates the magnetization vector towards its equilibrium direction, and the (negative) polarization process that builds up the z component of the magnetization towards its stationary state m_0^{st}.[9, 44] As shown by our experiments, one of the ingredients involved in the dynamics is the presence of a strong enough dipolar field in the sample to affect the evolution of the magnetization. Therefore, we next investigated these through a ensemble of simulations. In our numerical model, the dynamics can be studied by varying its strength through the (uniform) spin density m_o assigned to each moment on the lattice, the control parameter for this purpose.

In this series of simulations we assumed continuous a μw irradiation, which is part of model (B), with $\gamma_{n,ee} = 20.0$ Hz. Besides, the radiation damping time constant and the transverse relaxation rate γ_2 were set to the fixed value $\gamma_{rd} = 2.0$ kHz and $\gamma_2 = 650$ Hz, so that the ratio γ_{rd}/γ_2 was above unity, the theoretical maser threshold. Note that changing the value of m_o also affects the value of the radiation damping constant, so keeping γ_{rd} fixed in these simulations implied changing the parameter G in Equation 3 accordingly. The value of $\gamma_{n,ee} = 20.0$ Hz was chosen so as to mimic a buildup process that occurs on a much longer time scale than individual maser pulses, and therefore likely not interfering with the latter.

The effect of the DDF on the dynamics is presented in Figure 7, where the simulations

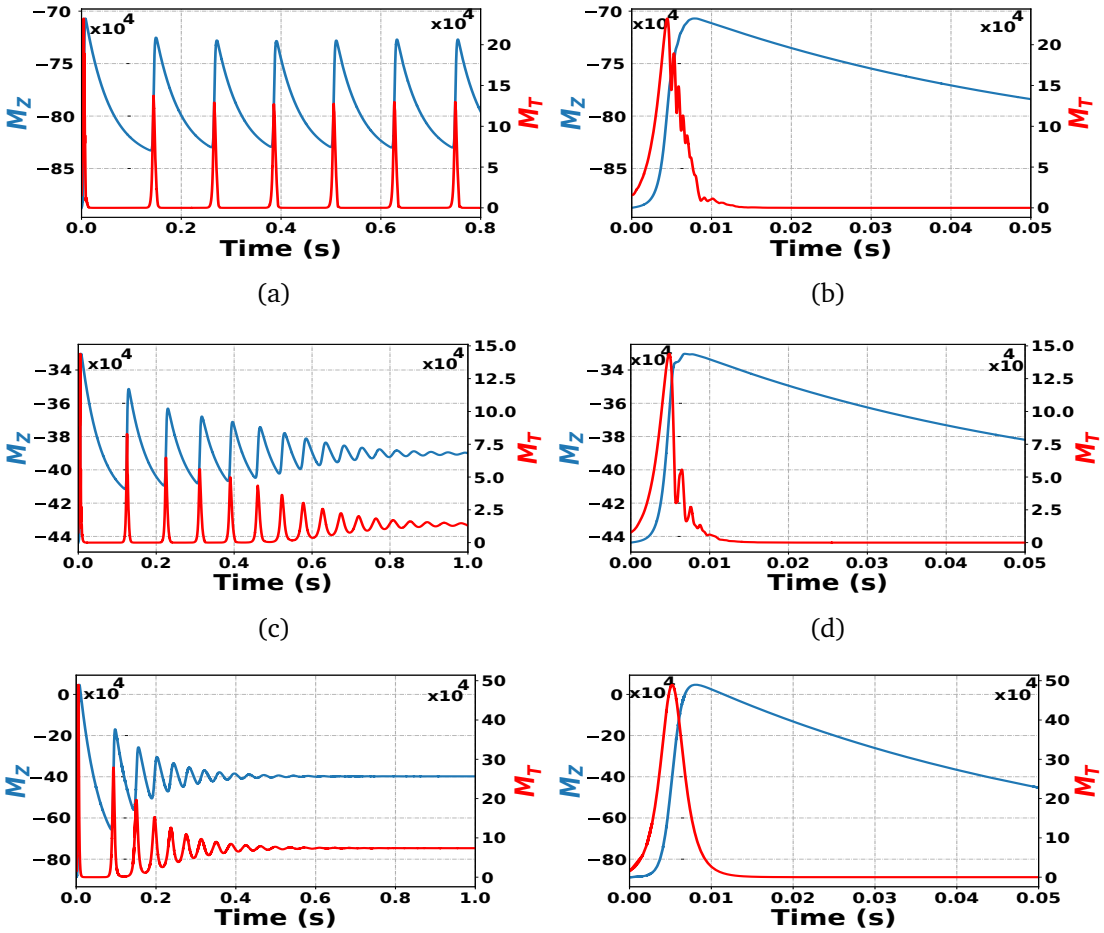

FIG. 7. Simulations of the effect of the DDF on the magnetization dynamics for Model (B). The envelope of the transverse magnetization $M_{\mathrm{T}} = \sqrt{m_x^2 + m_y^2}$ is depicted in red and the z component in blue. The strength of the dipolar field, measured by the frequency ω_{dip} is controlled by the magnetization density m_o. 7(a), 7(b) $\gamma_{rd}/\gamma_2 = 3.10$, $\omega_{dip}/\gamma_{rd} = 44.45$, $m_o = 400.0$ A/m 7(c), 7(d) $\gamma_{rd}/\gamma_2 = 3.10$, $\omega_{dip}/\gamma_{rd} = 22.22$, $m_o = 200.0$ A/m 7(e) 7(f) $\gamma_{rd}/\gamma_2 = 3.10$, and the distant dipolar interactions are absent. All simulations were performed with fixed values of the radiation damping time constant $\gamma_{rd} = 2.0k$ Hz, decay rate $\gamma_2 = 650$ Hz, and electron-nuclei equilibration rate $\gamma_{n,ee} = 20.0$ Hz. Simulations were performed on a disk-shaped sample.

show typical series of sustained maser bursts for different values of the spin density m_o. Interestingly, the envelope of the transverse signal shown in Figure 7(a) qualitatively reproduces the main features of the experiments, in which an apparent "steady-state" of regularly spaced masers was observed. Alternatively, in the simulations performed with decreasing values of m_o (from top to bottom), the intensities of the bursts monotonously decay and the transverse magnetization eventually reaches a constant intensity, indicating a steady-state precession about the z axis. Besides, the details of each maser pulse envelope are also affected. Indeed, one observes that for large values of m_o, each pulse

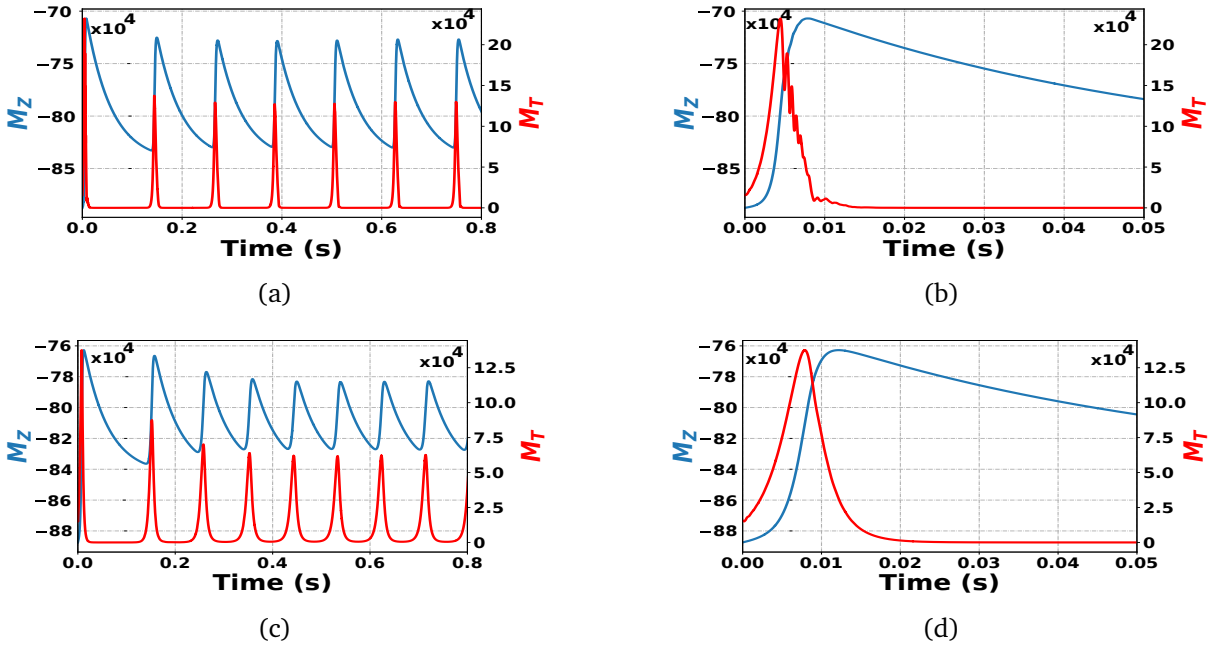

FIG. 8. Simulations of the magnetization dynamics for different values of the relaxation rate γ_2 and ratio γ_{rd}/γ_2 (Model B). 8(a), 8(b) $\gamma_{rd}/\gamma_2 = 3.10$ and $\gamma_2 = 650$ Hz; 8(c), 8(d) $\gamma_{rd}/\gamma_2 = 2.0$ and $\gamma_2 = 1.0$ kHz Simulations were performed for a disk-shaped sample and fixed values of the radiation damping time constant $\gamma_{rd} = 2.0k$ Hz, of $\gamma_{n,ee} = 20.0Hz$, and for a ratio $\omega_{dip}/\gamma_{rd} = 44.45$. The envelope of the transverse magnetization is depicted in red and the z component in blue.

exhibits an asymmetric profile with several pulses within it, whereas in the absence of any distant dipolar field, this "bursts within burst" pattern disappears, and the maser shape recovers the conventional symmetric, hyperbolic secant profile, as expected from the simpler BMP model used in previous work.[7, 9]

The effect of the decoherence rate γ_2 on the maser pulse dynamics was also investigated, and results are illustrated in Figure 8. Two such simulations, performed at constant γ_{rd} and m_0, therefore identical RD and DDF effects, and for different values γ_2 leading to $\gamma_{rd}/\gamma_2 = 3.1$ and $\gamma_{rd}/\gamma_2 = 2$, are shown. In both cases a continuous series of sustained maser are obtained. For larger γ_{rd}/γ_2 ratios, maser pulses are sharper and have shorter duration, which attests for a more efficient RD for longer transverse relaxation, a known and expected feature. This is associated with larger excursions of m_z during the pulses and larger the maximum excursion from its initial value (see Figure 8). Nevertheless, it is noteworthy that in all the simulations, the m_z component remains close to its initial value, within $\sim 79-86\%$ of its minimum, indicating that the trajectory of the magnetization vector lies in the proximity of the south pole of the Bloch sphere. Thus, with these parameters, the maser effect is actually rather inefficient, due to too

fast decoherence. Again, as shown in the previous example, the envelope of the maser pulse exhibits a clear asymmetry, with the presence of multiple, smaller, maser pulses within the main pulse. But for the lower γ_{rd}/γ_2 ratio, this asymmetry vanishes, suggesting that the presence of the faster decoherence prevents the distant dipolar field to significantly impact on the magnetization dynamics.

Sustained masers - the "cross-talk" situation We also performed numerical studies of model (A), which was introduced to mimics the magnetization dynamics of the ^{1}H nuclear spins in the presence of a ^{2}H reservoir. The presence of this additional nuclear spin reservoir allows for the repolarization of the former, both with and without μw irradiation, by an indirect "cross-talk" mechanism through the electron non Zeemann reservoir.[34, 35] In this case, only the ^{1}H spins are coupled to the detection circuit of the spectrometer, to which they lose energy, whereas the likewise hyperpolarized ^{2}H only exchange energy with other spins. As detailed in ref.[7] and explained above, this process leads to partial repolarization, i.e., re-cooling, from deuterium spins, together with a loss of polarization, therefore heating, of the ^{1}H nuclei. Thus, model (A) introduces a simplified description of this process, where the z magnetization $\mathbf{m}_z(\mathbf{r},t)$ tends to the value $\mathbf{m}_{0z}^{th}(\mathbf{r},t)$ that corresponds to the deuterium spin temperature, whilst deuterium spins itself relaxe to thermal equilibrium, in the absence of μw irradiation (see Eqs. 5 and 6).

In our simulations, the equilibrium magnetization m_o^{st} was set to $m_o^{st} = -0.05 \times \mathbf{m}_{oz}^{mw}$, where $\mathbf{m}_{oz}^{mw}$ represents the ^{1}H stationary (negative) magnetization upon microwave irradiation, and the initial state of the magnetization. Figure 9 shows simulations performed on an disk-shaped model sample. The model parameters were assigned the following values $m_o = 200$ A/m, $\gamma_2 = 650$ Hz, $\gamma_{rd} = 2$ kHz, so that $\gamma_{rd}/\gamma_2 = 3.1$ and $\omega_{dip}/\gamma_{rd} = 22.22$. In this model, the rates of return to the lattice temperature of the ^{2}H reservoir is set to $\gamma_{st} = 0.030$ Hz and the ^{1}H/^{2}H equilibration rate of spin temperatures is $\gamma_{n,ee} = 20$ Hz (see Eq; 6. During the early stage of the dynamics, the in-plane magnetization envelope exhibits a succession of a few ($\sim 7-8$) maser bursts of decaying intensities with time, until it reaches a long-term evolution of monotonous decay. Due to the presence of the dipolar field the asymmetry and the "bursts within burst" profiles are also reproduced. At longer evolution times the amplitude of the in-plane magnetization decays monotonously, whereas the z component of the magnetization returns to its thermal equilibrium value, in the absence of μw irradiation, with the γ_{st} time constant. These simulations thus reproduce satisfactorily the basic features of the

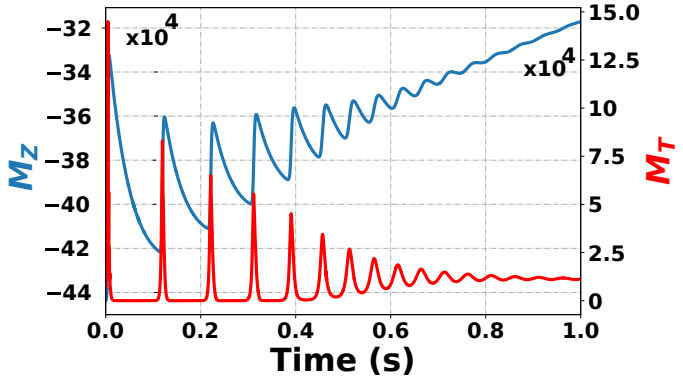

(a)

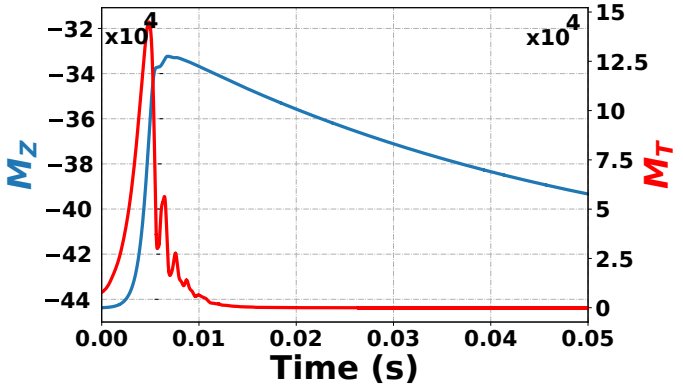

(b)

FIG. 9. Magnetization dynamics for DNP model (A) The envelope of the transverse magnetization is depicted in red and the z component in blue. 9(a) 9(b) $\gamma_{rd}/\gamma_2 = 3.10$, $\omega_{dip}/\gamma_{rd} = 22.22$ $\gamma_2 = 650Hz$, $\gamma_{rd} = 2.0$ kHz, $\gamma_{n,ee} = 20.0$ Hz and $\gamma_{st} = 0.030$ Hz. Calculations were performed for a disk-shaped sample (see text for details).

experimental observations described in Reference [7], i.e., asymmetric masers at short times and long lasting monotonous decay at long times.

IV. DISCUSSION

A. How to interpret the effect of the dipolar field on the dynamics

The work presented here aims at better understanding the complex non linear dynamics of a large magnetization subject to efficient radiation damping. To do so, the dynamical effects of the dipolar field were investigated through numerical simulations of a simplified model, which provided results that are consistent with several observed effects, both in this and previous work. In particular, it was found that for strong dipolar fields, the predicted evolution of the magnetization (Figures 7(a)) was similar to the observed one and depicted in Figures 2(a)-2(b), that is, a ”steady state” of regularly

spaced maser bursts. It is also noteworthy that in the absence of dipolar field, the model gives qualitatively the same predictions as the four-dimensional simplified BMP model introduced in Reference[7]. This transition is illustrated in Figure 7. It is also interesting that we were not able to reproduce the kind of long term evolution either with the simplified BMP model, or with the present lattice model without DDF. In our view, these elements strongly suggest that the kind of induction signal observed in this work attests for the presence of an effective DDF. The noted asymmetry and the "bursts within burst" profile are clearly also due to the presence of the DDF. However, the mechanism through which the dipolar field produces these effects is somewhat unclear. The dipolar field essentially contributes an average z component that is much larger than its transverse x and y components. The average $\langle\omega_{d,z}\rangle = -\langle B_{d,z}(\mathbf{r})\rangle/\gamma$ component is depicted in Figure 10 for a trajectory of model (B). It appears that its time evolution mirrors the M_z component of the magnetization, and therefore contributes a time-varying precession frequency to the magnetization. Considering its effect on an isolated burst, one would expect its effect to be that of a chirp pulse, with a time-varying offset frequency. However, the local dipolar field $\mathbf{B}_d(\mathbf{r}_i)$ at each site of the sample is not uniform, achieving a distribution of its z components, therefore of precession frequencies across the sample, as shown in Figure 10(b). From the dynamical viewpoint, this amounts to the existence of an inhomogeneity of B_0, albeit a time-dependent one. This is interesting, as it points to an effect that was already invoked in the context of solution NMR, where B_0 inhomogeneity was shown to lead to such non-decaying sustained maser pulses, an effect not explained by the Bloch-Maxwell equations.[45]

B. A comment on time scales

The simulations presented in this work qualitatively explain a number of features of the magnetization dynamics under DNP and radiation feedback conditions. The models introduced in this work involve a large number of parameters and time scales ($\gamma_{n,ee}, \gamma_{rd}, \gamma_{st}, \gamma_2$, shape of the sample and spin density) that control the kind of dynamics that the magnetization undergoes, and exploring the complete parameter space is a formidable task. We have restricted the study to ranges of parameters that were able to reproduce experimental observations and, as it turns out, some of them may seem remote from the experimental ones. Although these values were arbitrary to some extent, the important point made in our study are the roles played by the relative values

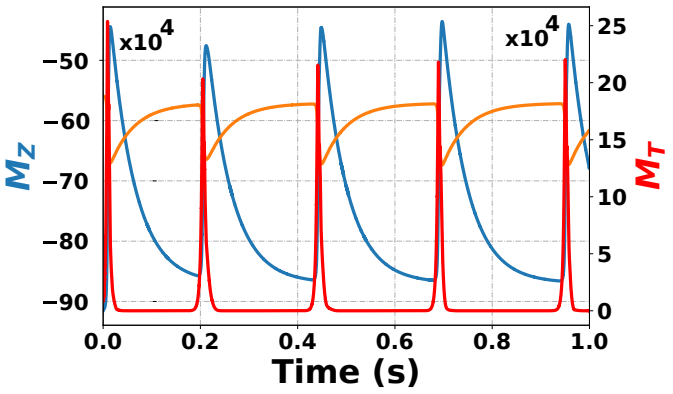

(a)

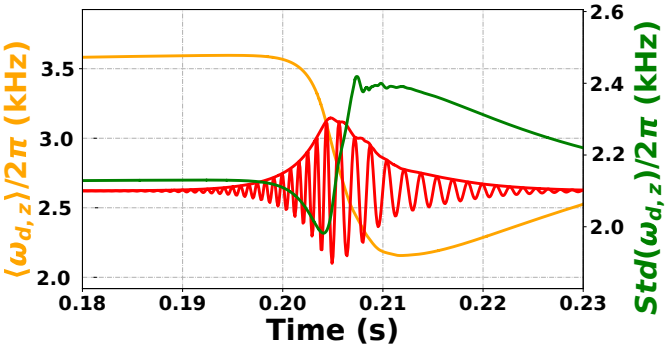

(b)

FIG. 10. Average and standard deviations of the dipolar field (z component). Simulations were performed for model B, with fixed values of the radiation damping time constants $\gamma_{rd} = 2.0$ kHz and $\gamma_{n,ee} = 20.0$ Hz. Simulations were performed on a cylindrical-shaped sample. In 10(a), the envelope of the transverse magnetization $M_{\mathrm{T}} = \sqrt{m_x^2 + m_y^2}$ is depicted in red and the z component in blue and the average $\langle\omega_{d,z}\rangle$ in orange. Simulations were performed for $\gamma_{rd}/\gamma_2 = 3.10$, $\omega_{dip}/\gamma_{rd} = 22.22$, $\gamma_2 = 650Hz$. In 10(b) the average $\langle\omega_{d,z}\rangle$ (orange), the standard deviation of $\omega_{d,z}$ (green), and the transverse magnetization are shown (the latter in arbitrary units).

of the ratios γ_{rd}/γ_2 and ω_{dip}/γ_{rd}: the former determines the maser threshold, whereas the latter controls the manifestation of DDF effects. Moreover, we have assumed a time scale separation between γ_{rd}, γ_2 and ω_{dip}, on the one hand, and on the much slower rates $\gamma_{n,ee}$ and γ_{st}, on the other hand. This corresponds to the much longer polarization buildup times.

Experimentally, one of the striking facts is that the observed duration of a typical maser pulse is on the order of ms to tens of ms despite the broad lines (~ 25 kHz). A crude analysis of the classical Bloch-Maxwell equations may lead to the erroneous conclusion that such a large relaxation rate γ_2 necessarily implies very narrow maser bursts. However, this is not necessarily true, as can be understood from the analysis made by Bloom[31] of radiation damping in the absence of T_1 relaxation. Indeed,

analytical solutions derived there show that the duration of a single maser pulse can actually be long. This can be seen from the relation between the radiation damping rate in the presence and in the absence of transverse relaxation, γ_{rd} and γ_{rd}^{∞}:[31]

$$\frac{\gamma_{rd}}{\gamma_{rd}^{\infty}} = \sqrt{\left(\frac{\gamma_2}{\gamma_{rd}^{\infty}}\right)^2 + 2\cos\theta_0 \frac{\gamma_2}{\gamma_{rd}^{\infty}} + 1} \tag{13}$$

where θ_0 is the initial flip angle. Then, for ratios $\frac{\gamma_2}{\gamma_{rd}^{\infty}} = 1 + \epsilon$ larger but close to unity, and for flip angles close to π, $\theta_0 = \pi - h$ so that $\cos\theta_0 = -\cos h = 1 - \frac{h^2}{2}$ to first order, one sees that the ratio of Equation 13 can be made arbitrarily small, meaning that $\gamma_{rd} \ll \gamma_{rd}^{\infty}$. This is illustrated in Figure11 This allows to explain why, even for very broad lines such as the ones in our experiments ($\sim$ 25 kHz), for extremely small flip angles and a radiation damping rate that is almost equal to the line width, maser bursts lasting tens of ms are observed. In fact, this situation was met experimentally when monitoring the polarization buildup with small pulses that trigger the DNP-NMR maser when the growing magnetization approaches the condition $\gamma_2 \approx \gamma_{rd}$. And although the simulations of Figure 11 were performed for the simple situation of a single maser pulse, they support the non intuitive magnetization dynamics in the more complex situation where radiation damping and the distant dipolar field are preent.

In our simulations, we have used values of γ_2 that are much lower than what the experimental line widths suggest ($\sim$ 25 kHz). This was imposed by numerical issues and we were not able to perform simulations with such large γ_2 and the required small flip angles values. However, based on the above discussion, we argue now that this does not affect the relevance of our calculations that provide insight into these complex phenomena.

C. Sample shape

Because it is determined by a large nonlinear differential system that, moreover, depends on many parameters, a complete exploration of the magnetization dynamics defined by the models of the DNP NMR maser proposed in this work is a formidable task. Nevertheless, we here illustrate by dynamics simulations the effect of the shape of the sample on the DDF, and on the magnetization dynamics. We considered the dynamics of model (A) for a specimen with the shape of a flat disk or an elongated cylinder. Results are depicted in Figure 12). Simulations were performed with identical

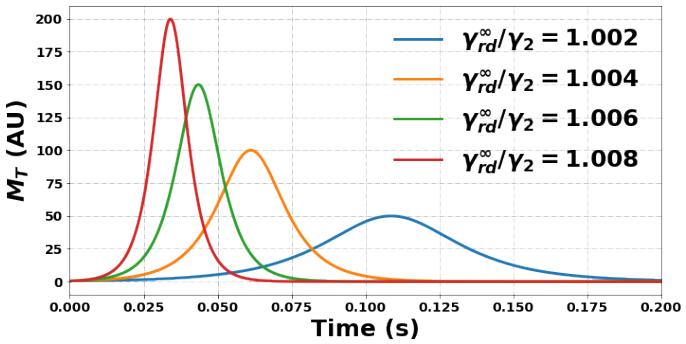

FIG. 11. Dependence of a single maser time duration on the $\gamma_{rd}^{\infty}/\gamma_2$ ratio, for a fixed flip angle $\theta = 179.999^o$, in the Bloom model[31]. The curves were obtained from Equations (14) in [31], with $\gamma_2 = 25$ kHz. For ratios approaching unity, the duration increases roughly a tenfold.

parameter values to show the pure effect of the sample shape on the dynamics. They show similar behaviors, with at short times, the series of maser bursts, followed by a transient stage of sustained precession in the intermediate region, and an evolution towards thermal equilibrium in the long term, when no significant radiation damping is present. However, the details of the maser pulses , in particular, are different, and can be ascribes to the different values of the DDF, therefore of the ω_{dip}/γ_{rd} ratios due to the different shapes of the samples. Nevertheless, as expected, the overall characteristics of the dynamics are conserved.

V. CONCLUSIONS

In this paper, we have presented an experimental and numerical analysis of a ^{1}H DNP-NMR maser operating at 1.2 K. The unexpected experimental observations of distant dipolar field effects in this context can be explained by the presence of an efficient radiation feedback that leads to a persistent coherence of the magnetization on time scales of seonds or minutes. An analysis based on a classical model taking into account radiation feedback from the probe and the presence of a dipolar field, together with a simplified model for DNP polarization provided sound description of this complex process.

CONFLICTS OF INTEREST

There are no conflicts of interest to declare.

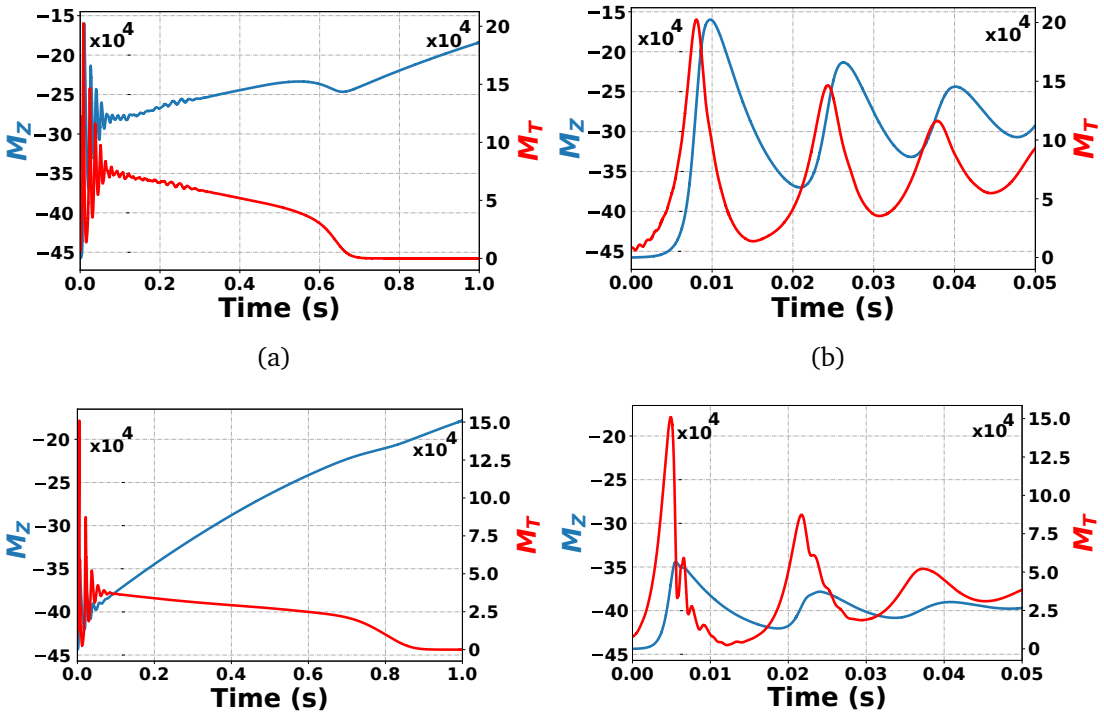

FIG. 12. Magnetization dynamics for DNP model (A) computed with $\gamma_2 = 650Hz$, $\gamma_{rd} = 2.0kHz$ ($\gamma_{rd}/\gamma_2 = 3.10$), $\gamma_{n,ee} = 151.5Hz$ and $\gamma_{st} = 1.0$ Hz, for 12(a) 12(b) an elongated cylinder with $\omega_{dip}/\gamma_{rd} = 11.11$; and 12(c) 12(d) a disk-shaped sample $\omega_{dip}/\gamma_{rd} = 22.22$.

ACKNOWLEDGEMENTS

The authors acknowledge Bruker BioSpin for providing a prototype of the DNP equipment, and the Très Grand Centre de calcul du (TGCC) for providing computation time.

This research was funded, in whole or in part, by the Agence Nationale pour la Recherche (ANR), Grant ANR-22-CE29-0006-01 - DynNonlinPol]. A CC-BY public copyright license has been applied by the authors to the present document and will be applied to all subsequent versions up to the Author Accepted Manuscript arising from this submission, in accordance with the grant's open access conditions.

[1] N. Bloembergen and R. V. Pound, *Phys. Rev.*, 1954, **95**, 8–12.

[2] A. Vlassenbroek, J. Jeener and P. Broekaert, *The Journal of Chemical Physics*, 1995, **103**, 5886–5897.

[3] A. Louis-Joseph, D. Abergel and J.-Y. Lallemand, *Journal of Biomolecular NMR*, 1995, **5**, 212–216.

[4] P. Broekaert and J. Jeener, *J. Magn. Reson. A*, 1995, **113**, 60.

[5] C. Anklin, M. Rindlisbacher, G. Otting and F. H. Laukien, *J. Magn. Reson. B*, 1995, **106**, 199.

[6] P. Bösiger, E. Brun and D. Meier, *Phys. Rev. Lett.*, 1977, **38**, 602–605.

[7] E. M. M. Weber, D. Kurzbach and D. Abergel, *Phys. Chem. Chem. Phys.*, 2019, **21**, 21278–21286.

[8] M. A. Hope, S. Björgvinsdóttir, C. P. Grey and L. Emsley, *The Journal of Physical Chemistry Letters*, 2021, **12**, 345–349.

[9] P. Bösiger, E. Brun and D. Meier, *Phys. Rev. A*, 1978, **18**, 671–684.

[10] V. Atsarkin, *Soviet Physics Uspekhi*, 1978, **21**, 725–745.

[11] A. Abragam and M. Goldman, *Reports on Progress in Physics*, 1978, **41**, 395–467.

[12] B. N. Provotorov, *Soviet Physics JETP*, 1962, **14**, 1126–1131.

[13] B. N. Provotorov, *Soviet Physics JETP*, 1962, **15**, 611–614.

[14] A. Vlassenbroek, J. Jeener and P. Broekaert, *Journal of Magnetic Resonance, Series A*, 1996, **118**, 234–246.

[15] J. Jeener, in *Dipolar Field and Radiation Damping: Collective Effects in Liquid-State NMR*, John Wiley & Sons, Ltd, 2007.

[16] A. Abragam, *Principles of Nuclear Magnetism*, Clarendon Press, Oxford, 1961.

[17] C. Slichter, *Principles of Nuclear Magnetic Resonance, third edition*, Springer-Verlag, 1989.

[18] G. Deville, M. Bernier and J. M. Delrieux, *Physical Review B*, 1979, 5666.

[19] Y.-Y. Lin, N. Lisitza, S. Ahn and W. S. Warren, *Science*, 2000, **290**, 118.

[20] J. Jeener, *Physical Review Letters*, 1999, **82**, 1772.

[21] V. Henner, H. Desvaux, T. Belozerova, D. J.-Y. Marion, P. V. Kharebov and A. R. Klots, *The Journal of chemical physics*, 2013, **139 14**, 144111.

[22] K. L. Sauer, F. Marion, P. J. Nacher and G. Tastevin, *Phys. Rev. B*, 2001, **63**, 184427.

[23] H. T. Edzes, *J. Magn. Reson.*, 1990, **86**, 293–303.

[24] A. Vlassenbroek, J. Jeener and P. Broekaert, *Journal of Magnetic Resonance A*, 1996, **118**, 234–246.

[25] A. Abragam, M. Chapellier, J. Jacquinot and M. Goldman, *Journal of Magnetic Resonance (1969)*, 1973, **10**, 322–346.

[26] H. Johannesson, S. Macholl and J. H. Ardenkjaer-Larsen, *J. Magn. Reson.*, 2009, **197**, 167–175.

[27] A. Abragam and M. Goldman, *Nuclear magnetism: order and disorder*, Clarendon Press, 1982.

[28] Y. Roinel and V. Bouffard, *J. Magn. Reson.*, 1975, **18**, 304–319.

[29] J. D. Walls, F. K. H. Phoa and Y.-Y. Lin, *Phys. Rev. B*, 2004, **70**, 174410.

[30] D. Abergel and J.-Y. Lallemand, *J. Magn. Reson. A*, 1994, **110**, 45.

[31] S. Bloom, *Journal of Applied Physics*, 1957, **28**, 800–805.

[32] J. R. B. Alan V. Oppenheim, Ronald W. Schafer, *Discrete-time Signal Processing*, Prentice Hall, 1999.

[33] T. Enss, S. Ahn and W. S. Warren, *Chemical Physics Letters*, 1999, **305**, 101–108.

[34] V. B. S F J Cox and M. Goldman, *J. Phys. C*, 1973, **6**, L100–L103.

[35] D. Guarin, S. Marhabaie, A. Rosso, D. Abergel, G. Bodenhausen, K. Ivanov and D. Kurzbach, *Journal of Physical Chemistry Letters*, 2017, **8**, 5531–5536.

[36] B. R. et al., 2022.

[37] M. Guéron, *Magn. Reson. Med.*, 1991, **19**, 31–41.

[38] M. Goldman, *Spin temperature and nuclear magnetic resonance in solids*, Clarendon Press, 1970.

[39] T. Wenckebach, *Essentials of Dynamic Nuclear Polarization*, Spindrift Publications, 2016.

[40] Y. Hovav, A. Feintuch and S. Vega, *Phys. Chem. Chem. Phys.*, 2013, **15**, 188–203.

[41] W. T. Wenckebach, *J. Magn. Reson.*, 2017, **277**, 68–78.

[42] S. P. N. Ernst Hairer, Gerhard Wanner, *Solving Ordinary Differential Equations I: Nonstiff Problems*, Springer, Berlin, Heidelberg, 1993.

[43] P. Virtanen, R. Gommers, T. E. Oliphant, M. Haberland, T. Reddy, D. Cournapeau, E. Burovski, P. Peterson, W. Weckesser, J. Bright, S. J. van der Walt, M. Brett, J. Wilson, K. J. Millman, N. Mayorov, A. R. J. Nelson, E. Jones, R. Kern, E. Larson, C. J. Carey, İ. Polat, Y. Feng, E. W. Moore, J. VanderPlas, D. Laxalde, J. Perktold, R. Cimrman, I. Henriksen, E. A. Quintero, C. R. Harris, A. M. Archibald, A. H. Ribeiro, F. Pedregosa, P. van Mulbregt and SciPy 1.0 Contributors, *Nature Methods*, 2020, **17**, 261–272.

[44] E. M. M. Weber, G. Sicoli, H. Vezin, G. Frébourg, D. Abergel, G. Bodenhausen and D. Kurzbach, *Angew. Chem. Int. Ed.*, 2018, **57**, 5171–5175.

[45] D. Abergel, A. Louis-Joseph and J.-Y. Lallemand, *Journal of Chemical Physics*, 2002, **116**, 7073–7080.